NASA TECHNICAL NOTE

NASA TN D-7557

RESEARCH TURBINE FOR HIGH-TEMPERATURE CORE ENGINE APPLICATION

I - Cold-Air Overall Performance of Solid Scaled Turbine

by Edward M. Szanca, Harold J. Schum, and Glen M. Hotz

Lewis Research Center
Cleveland, Ohio 44135

NATIONAL AERONAUTICS AND SPACE ADMINISTRATION • WASHINGTON D. C. • FEBRUARY 1974

RESEARCH TURBINE FOR HIGH-TEMPERATURE CORE ENGINE APPLICATION

I - COLD-AIR OVERALL PERFORMANCE OF SOLID SCALED TURBINE

by Edward M. Szanca, Harold J. Schum, and Glen M. Hotz

Lewis Research Center

SUMMARY

The cold-air performance of a half-scale model of a 50.8-centimeter (20-in.) turbine suitable for high-temperature "core" engine application is presented herein. The physical characteristic features of this turbine are low aspect ratio, thick leading and trailing edges, low solidity, and large relative rotor radial clearances.

The performance parameters presented herein are expressed in equivalent terms for an uncooled version (solid vanes and blades) of the aforementioned turbine.

Two rotor configurations were designed and tested. The first had untwisted rotor blades with the same aerodynamic profile from hub to tip to facilitate the fabrication of cooled blades utilizing complex cooling schemes. The second had twisted rotor blades designed for free-vortex flow and simple radial equilibrium. The second turbine was tested to determine the performance penalty incurred by using untwisted blades. Both turbines were tested over a range of speeds from 40 to 110 percent of design and inlet- to exit-total pressure ratios from about 1.4 to 2.8. Over the entire range of speeds and pressure ratios tested, the efficiency of the turbine with the twisted rotor blades was greater than the efficiency of the turbine with the untwisted rotor blades. At the design specific work output of 39.572 joules per gram (17.00 Btu/lbm) which occurred at a pressure ratio of 1.817, the total efficiency of the turbine with untwisted rotor blades was 87.1 percent. At this pressure ratio the efficiency of the turbine with twisted rotor blades was 88.0 percent. These results compare favorably with the design efficiency of 87.0 percent.

INTRODUCTION

Many future engines will be of the turbofan variety having high bypass ratios and high pressure and temperature "core" engine turbines. These turbines are characterized by their relatively small-sized blading (high hub- to tip-radius ratio) and low aspect ratio.

both of which are considered detrimental to turbine efficiency.

Research studies are presently being conducted at the Lewis Research Center to build a 50.8-centimeter- (20-in.-) diameter, single-stage turbine to operate at stoichiometric combustion (2478 K; 4000° F) and a turbine inlet pressure of 413.7 N/cm^2 abs (600 psia). At this temperature level, significant amounts of coolant flow are required. The turbine design will incorporate full-film cooled vanes, blades, and end walls. The introduction of these large amounts of cooling air into the main or primary flow stream can result in a significant deleterious effect on the turbine aerodynamic performance.

Prior to testing at the extremely high inlet-air conditions, candidate vane and blade designs will be tested in detail at much reduced inlet conditions in order to determine the aerodynamic effect of coolant air. To establish a basis of comparison, then, a solid (uncooled) version of the "core" turbine was fabricated. The purpose of the subject report is to present the design and test results of this turbine. The turbine investigated was a half-scale model of the design turbine, and had a rotor tip diameter of 25.4 centimeters (10 in.), with blade heights of 1.905 centimeters (0.75 in.), with no radial-axial flare. The rotor blades had a constant section profile from hub to tip and no twist. This type of design facilitates fabrication of complex blades and inserts. Use of untwisted rotor blading probably results in a turbine performance penalty, however. Accordingly, a second rotor was fabricated, designed for free-vortex flow and simple radial equilibrium, resulting in blade twist from hub to tip. This rotor was also tested with the same stator as used for the untwisted rotor, in order to determine the extent of the performance penalty.

Both the untwisted and the twisted turbines were tested at an inlet pressure of 17.237 N/cm^2 abs (25.0 psia) and an inlet temperature of approximately 306 K (550° R) and over a range of pressure ratio and speed. This report presents the performance in terms of equivalent mass flow, equivalent torque, equivalent specific work output, equivalent speed, outlet flow angle, and efficiency.

SYMBOLS

A area, cm^2; ft^2

b vane or blade height, cm; in.

c chord length, cm; in.

D diameter, cm; in.

g force-mass conversion constant, 1.0 (32.174 ft/sec^2)

Δh specific work, J/g; Btu/lbm

i rotor inlet relative incidence angle, deg

J mechanical equivalent of heat, 1.0 (778.16 ft-lb/Btu)

N turbine shaft speed, rad/sec; rpm

p pressure, N/cm^2 abs; psia

R gas constant, 287 J/(kg) (K); 53.34 ft-lb/(lb) (^{o}R)

r radius, cm; in.

s pitch cm; in.

T absolute temperature, K; ^{o}R

U blade velocity, m/sec; ft/sec

V absolute gas velocity, m/sec; ft/sec

W relative gas velocity, m/sec; ft/sec

w mass flow, kg/sec; lbm/sec

α absolute gas flow angle measured from the axial direction, deg

γ ratio of specific heats

δ ratio of inlet total pressure to U.S. standard sea-level pressure, p'_0/p^*

ϵ function of γ used in relating parameters to those using air inlet conditions at U.S. standard sea-level conditions, $\frac{\gamma^*}{\gamma}\left[\left(\frac{\gamma+1}{2}\right)^{\gamma/(\gamma-1)}\Big/\left(\frac{\gamma^*+1}{2}\right)^{\gamma^*/(\gamma^*-1)}\right]$

η total efficiency (based on inlet-total to exit-total pressure ratio)

θ_{cr} squared ratio of critical velocity at turbine inlet to critical velocity at U.S. standard sea-level air $\left(V_{cr}/V^*_{cr}\right)^2$

τ torque, N-m; ft-lb

Subscripts:

cr condition corresponding to Mach number of unity

b blade

h hub section

m mean section

t tip section

u tangential component

v vane

x axial component

0 station at turbine inlet (fig. 8)

1 station at stator exit (fig. 8)

2 station at turbine exit (fig. 8)

Superscripts:

' absolute total state

* U.S. standard sea-level conditions (temperature equal to 288.15 K (518.7° R), pressure equal to 10.13 N/cm^2 abs (14.7 psia))

TURBINE DESCRIPTION

Design parameters for an advanced high-temperature single-stage air-cooled axial-flow "core" engine turbine are summarized in table I. Also shown are the corresponding

TABLE I. - TURBINE DESIGN OPERATING VALUES

Performance parameter	Hot engine conditions (ASTM-A-1/Air = 0.0435)	Air-equivalent conditions
Tip diameter, D_t, cm (in.)	50.8 (20.0)	25.4 (10.0)
Inlet total temperature, T'_0, K (°R)	2200 (3960)	288.2 (518.7)
Inlet total pressure, p'_0, N/cm^2 abs (psia)	386.1 (560.0)	10.13 (14.7)
Mass flow, w, kg/sec (lbm/sec)	63.82 (140.72)	1.207 (2.660)
Turbine rotative speed, N, rpm	16 687	12 388
Specific work output, $\Delta h'$, J/g (Btu/lbm)	287.25 (123.4)	39.572 (17.00)
Mean blade speed, U_m, m/sec (ft/sec)	410.6 (1347)	152.4 (500.0)
Inlet- to exit-total pressure ratio, p'_0/p'_2	----------	1.818
Total efficiency, η, percent	----------	0.87

air-equivalent design parameters for the half-scale uncooled model tested herein. The equivalent conditions were derived assuming no coolant-air effects.

The test-turbine stator was fabricated with untwisted vanes of constant mean-section profile, ignoring the relatively small amount of twist (about 3°) from hub to tip if designed for free-vortex conditions. The rotor blades were also of constant profile from hub to tip, with no twist. These blading profiles were designed to facilitate fabrication of complex internal cooling-air-distribution inserts for future cooled turbine tests. The subject investigation, however, was conducted using solid (uncooled) blades.

The velocity diagram evolved to meet the design aerodynamic requirements is shown

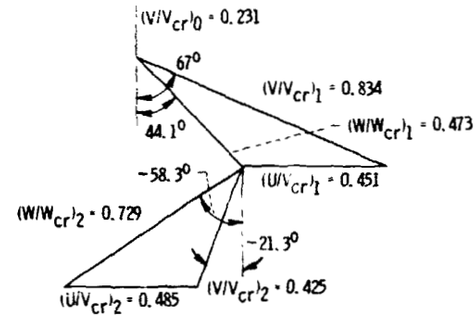

(a) Hub section; radius ratio $r_h/r_t = 0.850$.

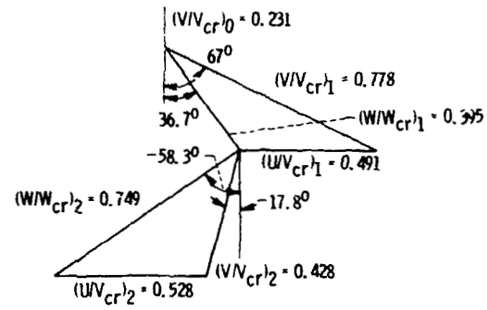

(b) Mean section; radius ratio $r_m/r_t = 0.925$.

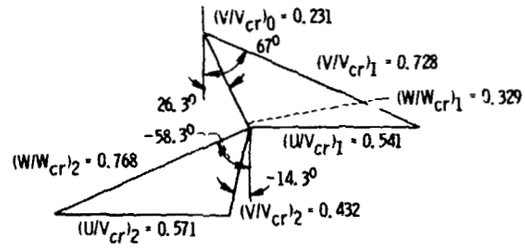

(c) Tip section; radius ratio $r_t/r_t = 1.000$.

Figure 1. - Turbine design velocity diagram.

in figure 1. All quantities represent the free stream uniform flow conditions. Pertinent test turbine geometry are presented in table II.

A second turbine, designed for the same requirements, was built and tested using the same vanes but employing twisted rotor blades as dictated from free-vortex and radial equilibrium considerations. All vanes and blades for the two turbine configurations are characterized by blunt leading and trailing edges, low aspect ratio, and high thickness to chord ratios. Because of the high rotor blade hub to tip ratio, the radial clearance (blade tip to casing) of 0.0432 centimeter (0.017 in.) represe about 2.3 percent of the blade height. All of these geometric factors are considered detrimental to high turbine effi-

TABLE II. - TEST TURBINE GEOMETRY

Stator	
Mean diameter, D_{mv}, cm (in.)	23.495 (9.25)
Vane height, b_v, cm (in.)	1.905 (0.75)
Axial chord, c_{xv}, cm (in.)	1.905 (0.75)
Axial solidity, $(c_{xv}/s_v)m$	0.929
Aspect ratio, b_v/c_x	1.000
Number of vanes	36
Leading edge radius, cm (in.)	0.254 (0.100)
Trailing edge radius, cm (in.)	0.0445 (0.0175)
Rotor	
Mean diameter, D_{mb}, cm (in.)	23.495 (9.25)
Blade height, b_b, cm (in.)	1.905 (0.75)
Axial chord, c_{xb}, cm (in.)	1.715 (0.675)
Axial solidity, $(c_{xb}/s_b)m$	1.652
Aspect ratio, b_b/c_{xb}	1.111
Number of blades	64
Tip clearance, cm (in.)	0.043 (0.017)
Leading edge radius, cm (in.)	0.1494 (0.0588)
Trailing edge radius, cm (in.)	0.0445 (0.0175)

ciency. The overall design efficiency of the turbine based on inlet- to exit-total pressure ratio was determined to be 87 percent. This efficiency was based on the value of mean speed-work parameter $U_m^2/gJ\,\Delta h$ of 0.587 and corrections found in the literature to account for the low aspect ratio, size effect due to scaling, and radial clearance. No correction was made for the incidence angle caused by the untwisted design since reference 1 indicates no significant loss with incidence from approximately -10° to approximately $+10^\circ$ (depending on the amount of reaction). For the subject turbine with untwisted rotor blades, the incidence angles were calculated to be $+7.4^\circ$ at the hub and -10.4° at the tip which are within the tolerance limits of reference 1.

Vane and rotor blade design surface pressure distributions at the mean section are shown in figures 2 and 3, respectively, calculated by the method of reference 2. Figure 2 shows a decreasing pressure drop on the suction surface of the vane from the leading edge to about 40 percent of the axial chord. From this point on the pressure ratio remains nearly constant up to about 85 percent of the chord length, at which point the pressure increases to the stator exit. In terms of velocity along the suction surface, this can be interpreted as an accelerating flow up to a value near the stator leaving velocity with some diffusion over the final portion of the suction surface. The low diffusion of the stator is considered favorable for high stator efficiency.

The pressure distribution along the pressure surface of the vane (fig. 2) is typical, with gradually decreasing pressure from leading edge to trailing edge.

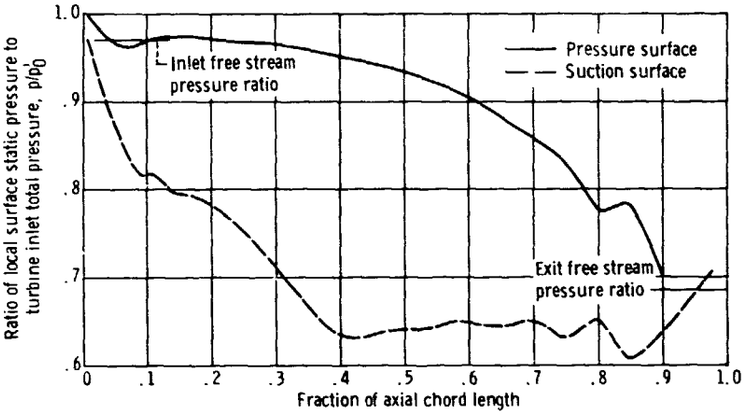

Figure 2. - Design surface static pressure distribution at stator mean section.

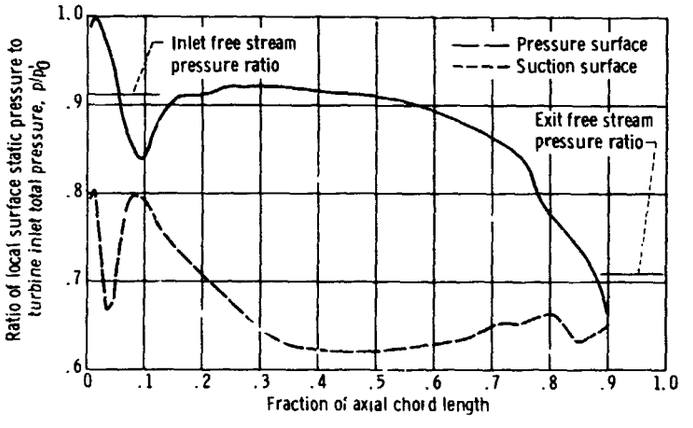

Figure 3. - Design surface static pressure distribution at rotor mean section.

Figure 3 shows a low pressure spike on the suction surface of the rotor blade near the leading edge. The sudden drop in pressure is caused by the accelerating flow around the leading edge of the blade. As the fluid passes around this circular leading edge, an abrupt change in curvature results in a deceleration of the flow and the resultant high pressure. After the leading edge the pressure along the suction surface drops to a pressure approximately equal to the rotor exit static pressure.

Along the pressure surface a pressure spike occurs for the same reasons as discussed for the suction surface. The spike, however, occurs further from the leading edge as measured along the axial chord than that for the suction surface. The result was an "hour-glass" pressure distribution near the forward portion of the blade.

Although it was not suspected that the low pressure spikes contributed to any appreciable loss, a more gradual transition in curvature from leading edge to blade surface

TABLE III - STATOR VANE COORDINATES

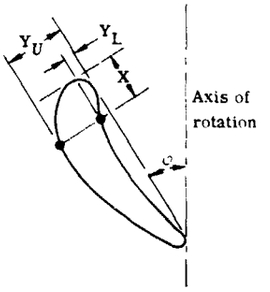

Mean Section					
Orientation angle, σ, deg					
$44^{o}37$					
X		Y_L		Y_U	
cm	in.	cm	in.	cm	in.
0	0	0.2540	0.100	0.2540	0.100
.064	.025	------	------	.4255	.1675
.127	.050	------	------	.5029	1980
.191	.075	------	------	.5613	.2210
.254	.100	------	------	.6071	.2390
.318	.125	------	------	.6439	.2535
.381	.150	.0318	.0125	.6731	2650
.445	.175	.0597	.0235	.6960	.2740
.508	.200	.0826	.0325	.7137	.2810
.572	.225	.1029	.0405	.7246	.2860
.635	.250	.1207	.04[illegible]	.7341	.2890
.699	.275	.1334	.0525	.7366	.2900
.762	.300	.1461	.0575	.7379	.2905
.889	.350	.1651	.0650	.7315	.2880
1.016	.400	.1803	.0710	.7163	.2820
1.143	.450	.1880	.0740	.6909	.2720
1.270	500	.1918	.0755	.6617	.2605
1.397	.550	.1905	.0750	.6287	.2475
1.524	.600	.1867	.0735	.5944	.2340
1.651	.650	.1765	.0695	.5550	.2185
1.778	.700	.161[illegible]	0650	.5156	.2030
1.905	.750	.1486	.0585	4724	.1860
2.032	.800	.1308	.0515	4255	.1675
2.159	.850	.1105	.0435	.3734	.1470
2.286	.900	.0902	.0355	3188	.1255
2.413	.950	.0660	.0260	.2591	.1020
2.540	1.000	.0406	.0160	.1956	.0770
2.667	1.050	.0127	.0050	.1295	.0510
2.776	1.093	.0445	.0175	.0445	.0175
		Stacking axis coordinates			
		x		y	
		cm	in.	cm	in.
		2.7318	1.0755	0.0445	0.0175

TABLE IV. - ROTOR BLADE COORDINATES

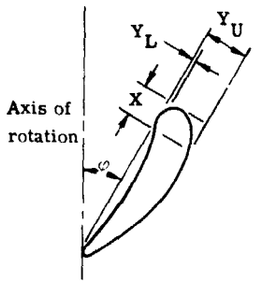

X		Hub section				Mean section				Tip section			
		Orientation angle, φ, deg											
		$17^{\circ}54'$				24°				$30^{\circ}13'$			
		Y_L		Y_U		Y_L		Y_U		Y_L		Y_U	
cm	in.	cm	in.	cm	in.	cm	in.	cm	in.	cm	in.	cm	in.
0	0	0.1494	0.0588	0.1494	0.0588	0.1494	0.0588	0.1494	0.0588	0.1494	0.0588	0.1494	0.0588
.064	.025	------	------	.3239	.1275	------	------	.3302	.1300	------	------	.3023	.1190
.127	.050	------	------	.4318	.1700	------	------	.4229	.1665	------	------	.3874	.1525
.191	.075	------	------	.5080	.2000	------	------	.4877	.1920	------	------	.4483	.1765
.254	.100	------	------	.5626	.2215	.0419	.0165	.5448	.2145	.0419	.0165	.4978	.1960
.381	.150	.1422	.0560	.6553	.2580	.1321	.0520	.6223	.2450	.1257	.0495	.5664	.2330
.508	.200	.2210	.0870	.7125	.2805	.2007	.0790	.6655	.2620	.1803	.0710	.6007	.2365
.635	.250	.2794	.1100	.7417	.2920	.2515	.0990	.6795	.2675	.2184	.0860	.6071	.2390
.762	.300	.3137	.1235	.7442	.2930	.2807	.1105	.6693	.2635	.2426	.0955	.5931	.2335
.889	.350	.3353	.1320	.7201	.2835	.2921	.1150	.6414	2525	2464	.0970	.5664	2230
1.016	.400	.3353	.1320	.6782	.2670	.2896	.1140	.6007	.2365	.2388	.0940	.5283	.2080
1.143	.450	.3175	.1250	.6236	.2455	.2718	.1070	.5486	.2160	.2210	.0870	.4801	.1890
1.270	.500	.2870	.1130	.5601	.2205	.2388	.0940	.4877	.1920	.1943	.0765	.4305	.1695
1.397	.550	.2413	.0950	.4890	.1925	.1956	.0770	.4191	.1650	.1575	.0620	.3747	.1475
1.524	.600	.1854	.0730	.4026	.1585	.1461	.0575	.3454	1360	.1168	.0460	.3099	.1270
1.651	.650	.1214	.0480	.3073	.1210	.0927	.0365	.2629	.1035	.0737	.0290	.2375	.0935
1.778	.700	.0533	.0210	.2032	.0800	.0356	.0140	.1715	.0675	.0279	.0110	.1575	.0620
1.905	.750	------	------	------	------	.0445	.0175	.0445	.0175	------	------	------	------
1.908	.751	------	------	------	------	------	------	------	------	.0445	.0175	.0445	.0175
1.975	.758	.0445	.0175	.0445	.0175	------	------	------	------	------	------	------	------
		Stacking axis coordinates											
		x		y		x		y		x		y	
		cm	in.	cm	in.	cm	in.	cm	in.	cm	in.	cm	in.
		0.810	0.319	0.386	0.152	0.772	0.304	0.361	0.142	0.742	0.292	0.328	0.129

C-71-4256

Figure 4. - Turbine stator.

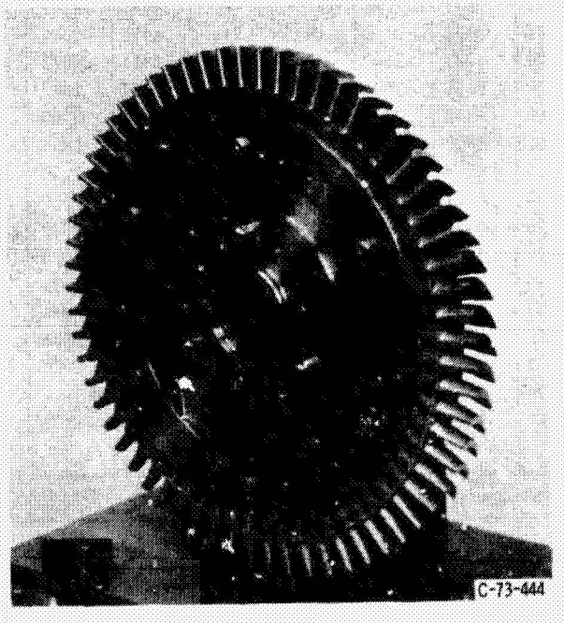

C-73-444

(a) Rotor with twisted blades.

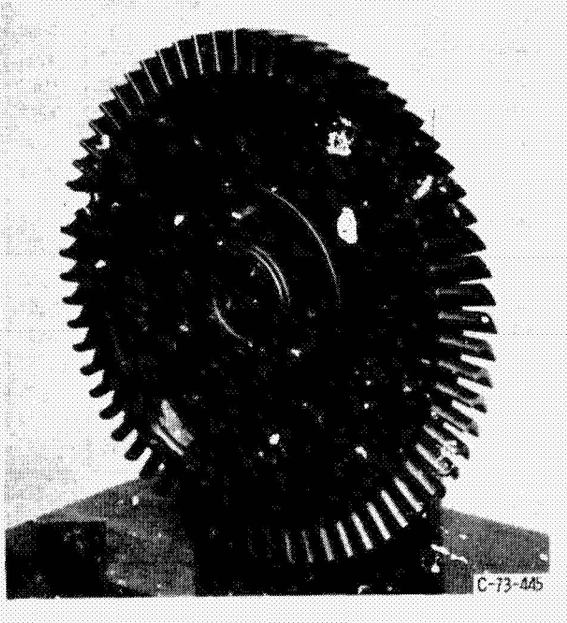

C-73-445

(b) Rotor with untwisted blades.

Figure 5. - Rotor with twisted and untwisted blades.

would improve the blade loading profile.

Vane profile coordinates are presented in table III; rotor blade coordinates at the hub, mean, and tip sections for the twisted configuration are given in table IV. For the untwisted rotor blade configuration, the mean section profile was maintained constant from hub to tip. All dimensions are for the half-scale test model. A photograph of the stator is presented in figure 4. Similarly, photographs of the twisted and the untwisted rotor assemblies are shown in figures 5(a) and (b), respectively.

APPARATUS

The apparatus consisted of the turbine as described in the preceding section, a speed-decreasing gear box, a cradled dynamometer, and an inlet and exhaust piping system with flow controls. A 223.7-kilowatt (300-hp) electric dynamometer was used to absorb the power output of the turbine, control its speed, and measure torque output. Both the gear box and the dynamometer were supported on hydrostatic bearings to minimize bearing friction losses. The arrangement of the experimental equipment is shown schematically in figure 6.

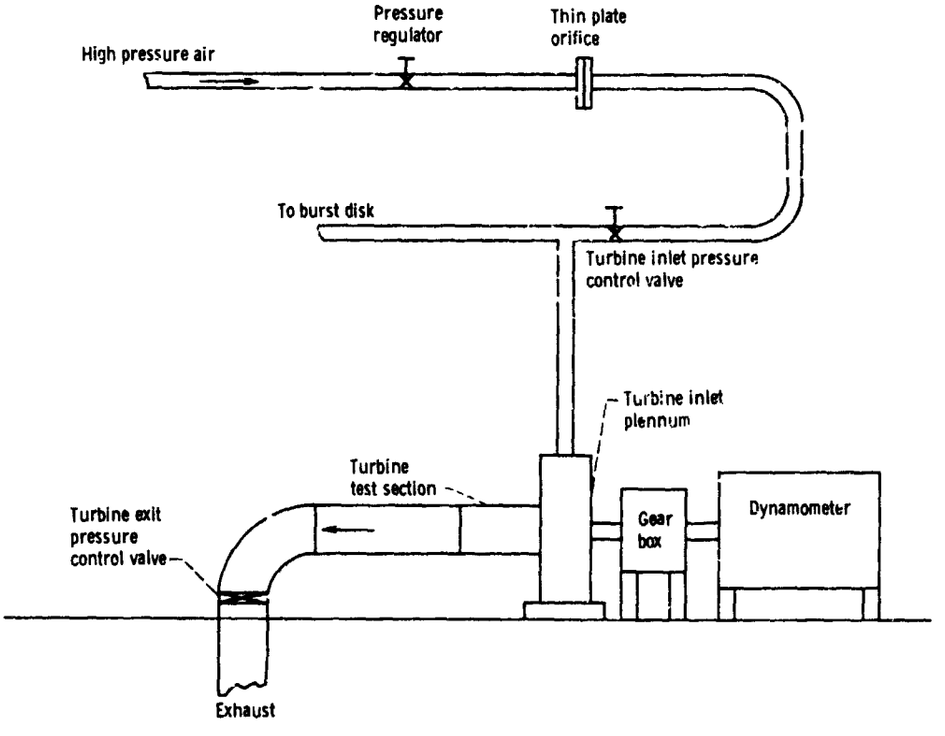

Figure 6. - Test installation schematic.

Pressurized air was filtered, metered by a calibrated flat-plate orifice and remotely throttled to the desired turbine inlet pressure. After the air had passed through the turbine, it was discharged into the laboratory altitude exhaust system. Turbine exhaust pressure was controlled by a remotely operated butterfly throttle valve in the exhaust piping. Figure 7 is a photograph of the test facility.

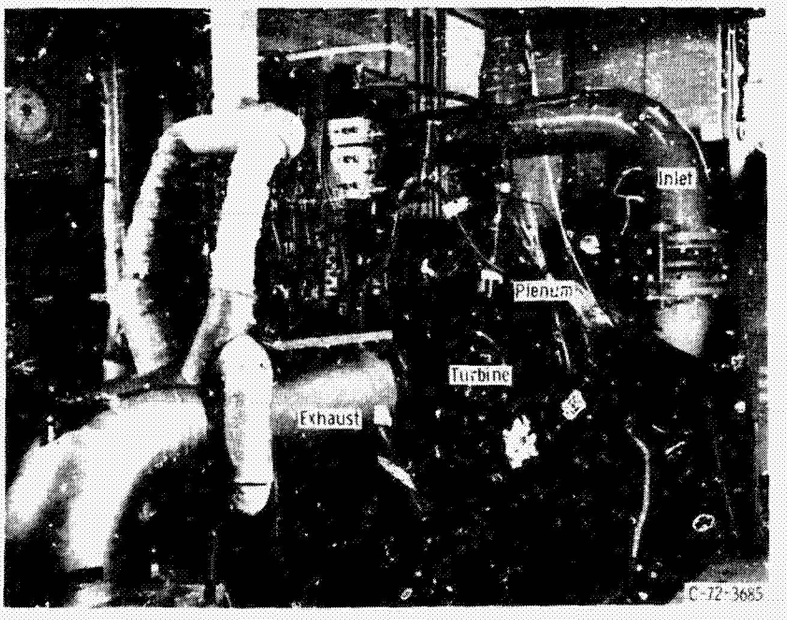

Figure 7. - Test facility.

INSTRUMENTATION

A schematic cross section of the turbine is shown in figure 8. Also shown on this figure are the instrument measuring stations.

At the turbine inlet (station 0), the instrumentation consisted of static pressure and total temperature sensors. The temperature was measured with three thermocouple rakes, each containing two thermocouples located at the area center radii of two equal annular areas. Static pressure was obtained from eight taps with four on the inner wall and four on the outer wall. The inner and outer taps were located opposite each other and were spaced 90° apart about the circumference.

The instrumentation at station 1, between the stator and the rotor, consisted of eight static pressure taps. These taps were spaced 90° apart with four on the inner wall and four on the outer wall as described for station 0. All static taps were located downstream

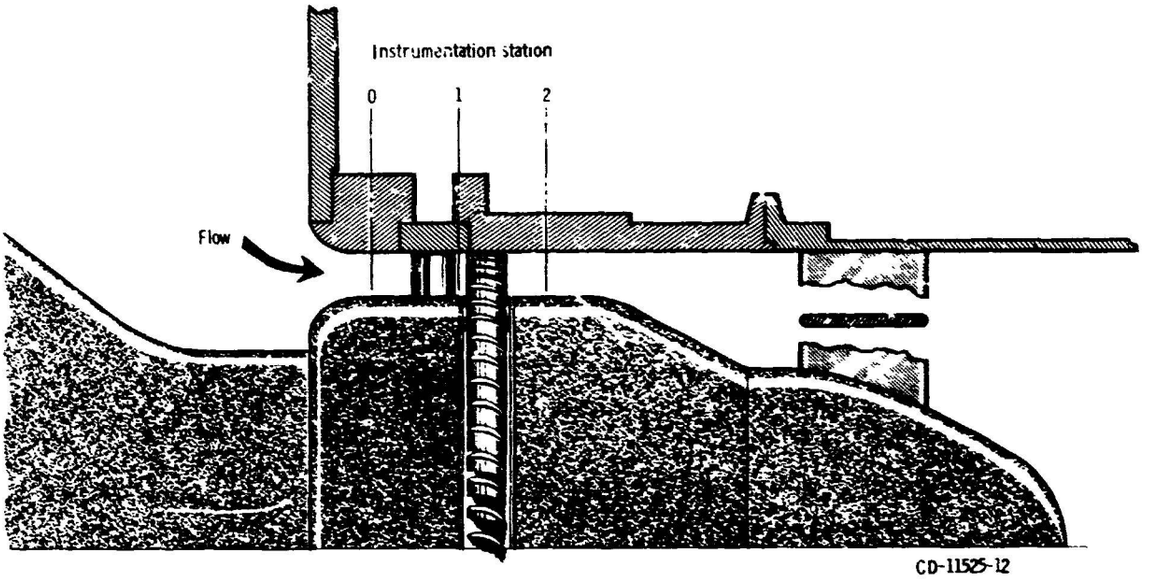

Figure 8. - Schematic of turbine test section.

of the stator-blade trailing edges, and in the center of the projected free stream channel.

The turbine outlet measuring station (station 2) was located about one blade chord downstream of the rotor. The instrumentation included static pressure, total pressure, total temperature, and flow angle. The static pressure was measured with eight wall taps located as described for station 0. The outlet flow angle was measured with an angle sensitive probe and a self-alining probe actuator. Also mounted on the angle measuring probe were provisions for determining total pressure. The angle and total pressure sensing elements were located at the mean blade height.

Turbine torque was transmitted to a commercial strain-gage load cell through a torque arm attached to the dynamometer stator. The rotational speed was detected by a magnetic pickup and shaft-mounted gear.

All pressures were measured with calibrated electrical transducers. A 200-channel data acquisition system was used to measure and record the electrical signals from the transducers.

PROCEDURE

Turbine performance with each rotor was obtained at nominal turbine inlet conditions of 17.237 N/cm^2 abs (25.0 psia) pressure and ambient temperature (approximately 306 K (550° R)). Data were obtained over a range of inlet- to exit-total pressure ratios from

1.4 to 2.8 and over an equivalent speed range from 40 to 110 percent of design.

Torque calibrations were obtained before and after each performance run. The calibrations were obtained with the dynamometer in the motoring mode, rotating the turbine at a speed of approximately 4500 rpm. Thus, most of the effects of bearing and seal friction were accounted in the calibration. Turbine windage losses were minimized during the calibrations by evacuating the air from the turbine housing.

The turbine efficiency was rated on the basis of inlet- to exit-total pressure ratio. Inlet and outlet total pressure were calculated from mass flow, static pressure, total temperature, and flow angle from the following equation:

$$p' = p\left\{\frac{1}{2} + \frac{1}{2}\left[1 + \frac{2(\gamma - 1)R}{\gamma g}\left(\frac{w\sqrt{T'}}{pA\cos\alpha}\right)^2\right]^{1/2}\right\}^{\gamma/(\gamma-1)}$$

At the inlet, the flow angle α was assumed to be axial ($\cos\alpha_0 = 1$). At the exit, the total temperature was computed from measured values of torque, mass flow, and inlet total temperature.

RESULTS AND DISCUSSION

The results of this investigation are presented in three parts. The first section covers the turbine performance obtained using a rotor with untwisted blades. The second section covers the performance obtained with twisted rotor blades. The third section is a comparison between the performance of the two turbine configurations to determine the effect of twist in the rotor blades. All data are shown in terms of equivalent air values. The experimental results include overall performance in terms of equivalent mass flow, equivalent specific work, and efficiency Also included are the variations in turbine exit flow angle and static pressure within the turbine.

Turbine Performance With Untwisted Rotor Blades

Overall performance. - The overall performance map for the turbine with untwisted rotor blades is shown in figure 9 in terms of specific work output $\Delta h/\theta_{cr}$ and a mass flow-speed parameter $\epsilon w\sqrt{\theta}/\delta$ for lines of constant total pressure ratio and equivalent rotor speed. Contours of constant values of efficiency based on the total pressure ratio across the turbine are also included.

The turbine design specific work output of 39.572 joules per gram (17.00 Btu/lbm) was obtained at a total pressure ratio of 1.817, and corresponds to an efficiency of 87.1 percent. This efficiency compares well to the 87 percent predicted efficiency. The map

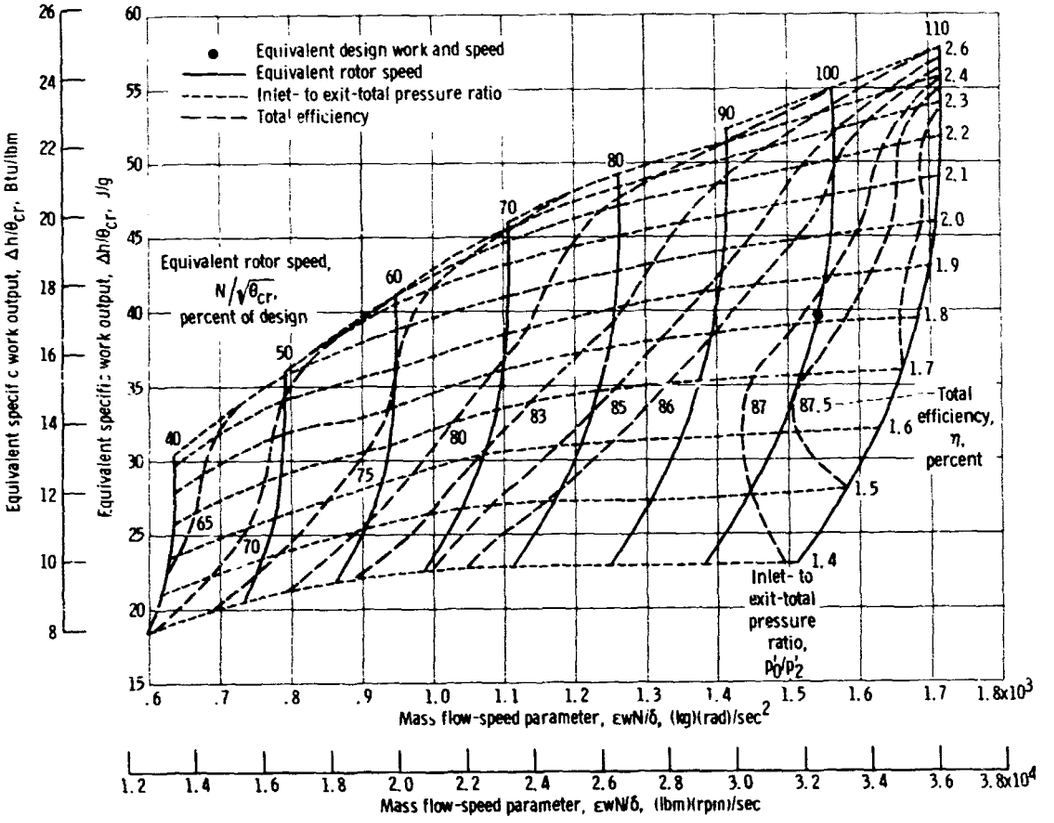

Figure 9. - Overall turbine performance map for turbine with untwisted rotor blades.

also shows that the design specific work is well below limiting loading indicating a conservative design.

Over the range of pressure ratios and speeds investigated, the turbine efficiency varied from about 65 percent near the 40 percent speed line, to 88 percent near the 110 percent speed line.

Stator mass flow calibration. - A mass flow calibration of the stator was made with the turbine rotor removed. This calibration was run over a range of pressure ratio (turbine inlet total to turbine exit tip static pressure p_0/p_{2t}) from 1.15 to 2.9. The variation in mass flow with pressure ratio is shown in figure 10. The choking mass flow for the stator was 1.233 kilograms per second (2.718 lbm/sec) and occurred at a pressure ratio p'_0/p_{2t} of 1.75. This flow was about 5 percent less than design, indicating a smaller throat area than designed.

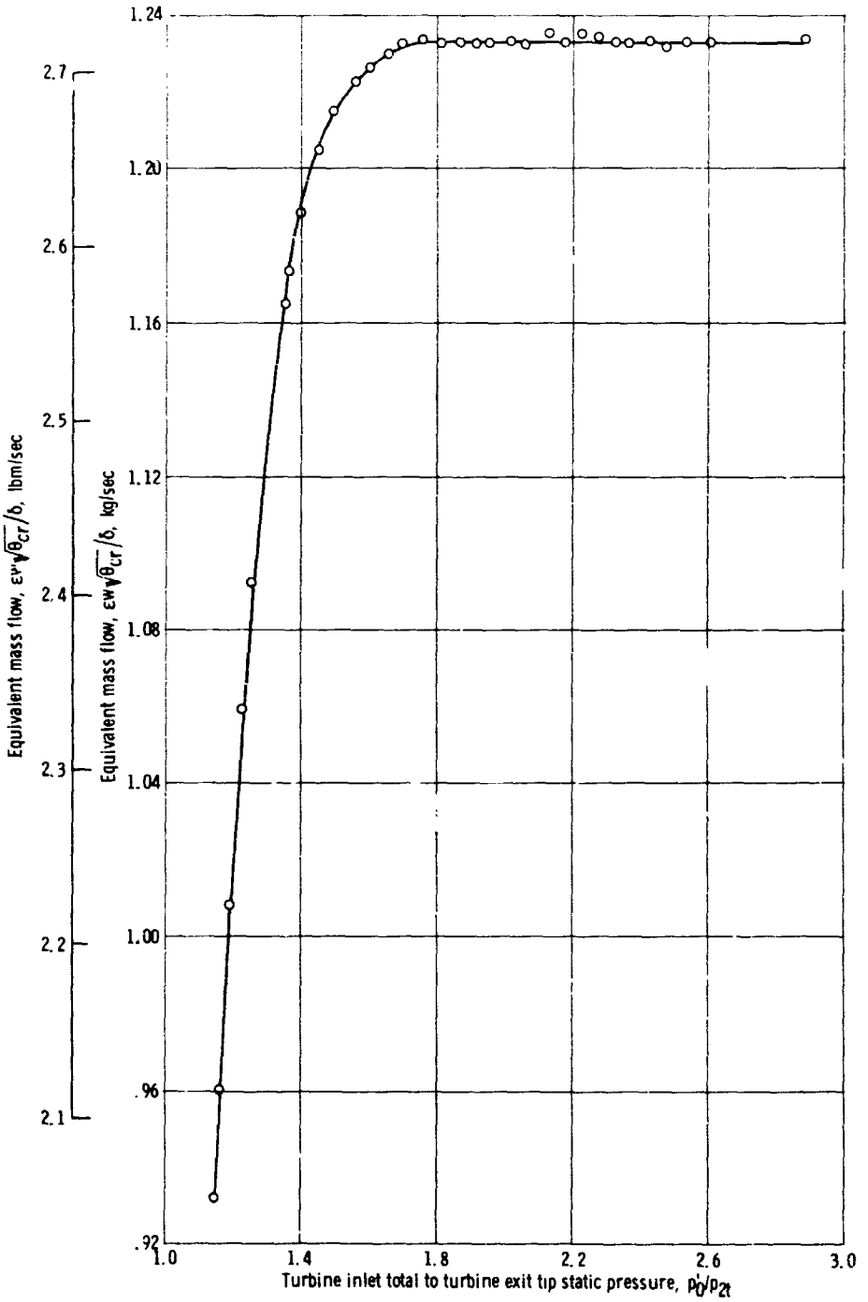

Figure 10. - Stator mass flow calibration.

orque and mass flow characteristics. - The variation of equivalent torque $\epsilon\tau/\delta$ and of equivalent mass flow $\epsilon w\sqrt{\theta_{cr}}/\delta$ with pressure ratio for the speeds investigated is shown in figures 11 and 12, respectively. Data from the faired curves of these two figures were used to calculate the performance map shown in figure 9.

The torque curves are typical and show that torque continually increased with increasing pressure ratio for all speeds over 50 percent design. At the design equivalent speed and a pressure ratio of 1.817, which corresponds to design specific work output,

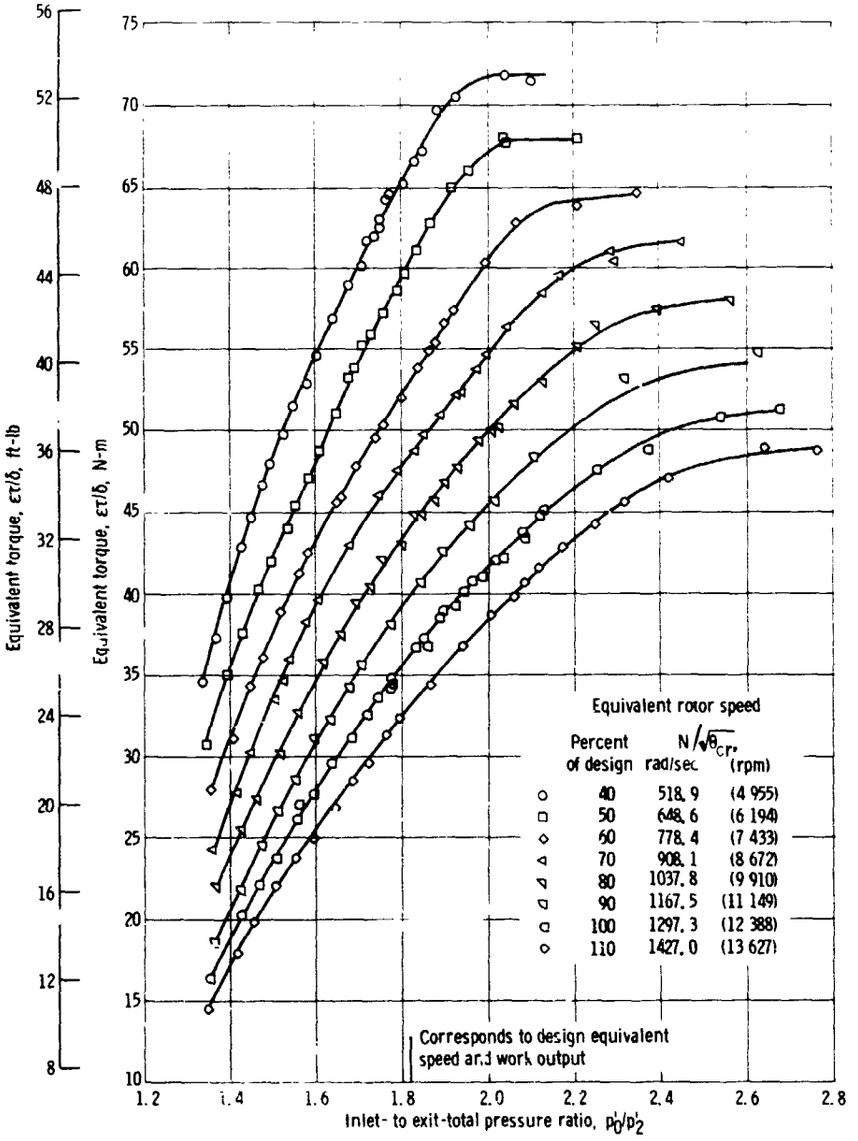

Figure 11. - Variation of torque with pressure ratio and speed for untwisted rotor blade configuration.

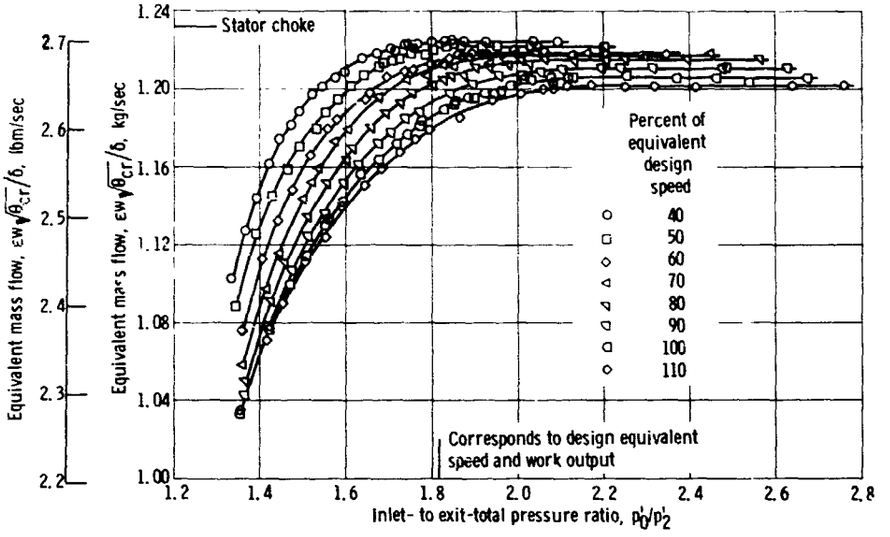

Figure 12. - Variation of mass flow with pressure ratio and speed for untwisted rotor blade configuration.

the equivalent torque was 36.133 newton-meters (26.65 ft-lb).

The equivalent mass flow of the turbine with the untwisted rotor blades is shown in figure 12 as a function of pressure ratio and speed. The separation of the speed lines in the figure indicates the flow is being controlled by the rotor. At 40 percent of equivalent design speed and the rotor choked at a total pressure ratio of 1.82 and flow of 1.225 kilograms per second (2.700 lbm/sec). As the speed was increased, the flow at any given pressure ratio decreased. At 110 percent of design speed, the rotor choked at a pressure ratio of 2.15 and a flow of 1.202 kilograms per second (2.650 lbm/sec).

At the design equivalent speed and at a pressure ratio of 1.817, which corresponds to the design specific work output of 39.572 joules per gram (17.00 Btu/lbm), the equivalent mass flow was 1.188 kilograms per second (2.620 lbm/sec) as compared to the design equivalent flow of 1.207 kilograms per second (2.660 lbm/sec).

Turbine-outlet flow angle and static pressure distribution. - The average flow angle at the turbine outlet is shown in figure 13 as a function of the speed and the total pressure ratio across the turbine. Negative angle data correspond to a positive contribution to work output. The average angle indicated at the conditions of equivalent design specific work output at equivalent design speed is -11.5° as compared to -17.8° at design. The smaller angle leaving the rotor indicates a lower swirl component of velocity leaving the rotor. Also, since ΔV_u must remain constant for a given design specific work and speed, the tangential component of velocity leaving the stator must be larger than designed. This was caused by a pressure drop across the stator greater than design and resulted in increasing the positive incidence angle into the rotor at design work and speed. The effect of incidence will be discussed in a later section where the performance

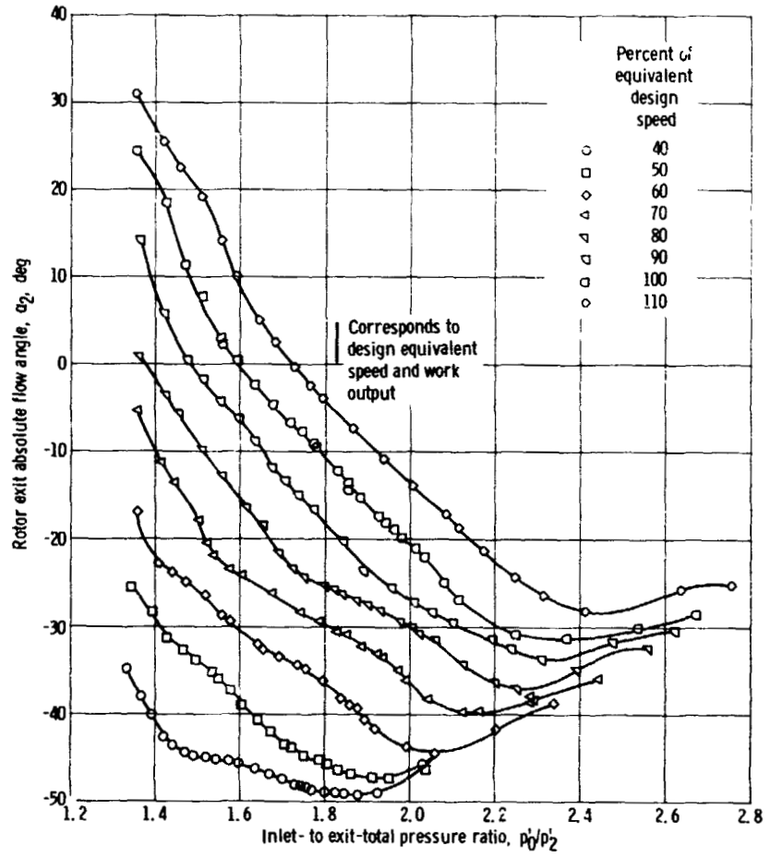

Figure 13. - Variation of turbine exit absolute flow angle with pressure ratio and speed for untwisted rotor blade configuration.

between the two rotor configurations is discussed.

The cause for the stator overexpansion can be partly attributed to higher rotor losses caused by the larger rotor radial clearance (percentage) of the scaled version turbine as compared to the 50.8-centimeter (20-in.) design turbine. Because of the mechanical limitations of the test facility, the ratio of radial clearance to annulus area of the scaled version was almost twice that of the 50.8-centimeter (20-in.) design turbine.

The variation in static pressure through the turbine is shown in figure 14 as a function of total pressure ratio for design speed. All pressures are ratioed to the inlet total pressure. The static measurements at the hub are shown in figure 14(a), tip measurements in figure 14(b). Choking in a blade row is indicated when the static pressure at the inlet to a blade row remains constant as the total pressure ratio across the turbine is increased. Referral to figures 14(a) and (b) shows that the hub and tip sections of the rotor choked at approximately the same overall total pressure ratio of 2.25. At choking conditions the pressure ratio to the rotor inlet at the hub was 0.55. The corresponding pressure ratio at the rotor tip was 0.61.

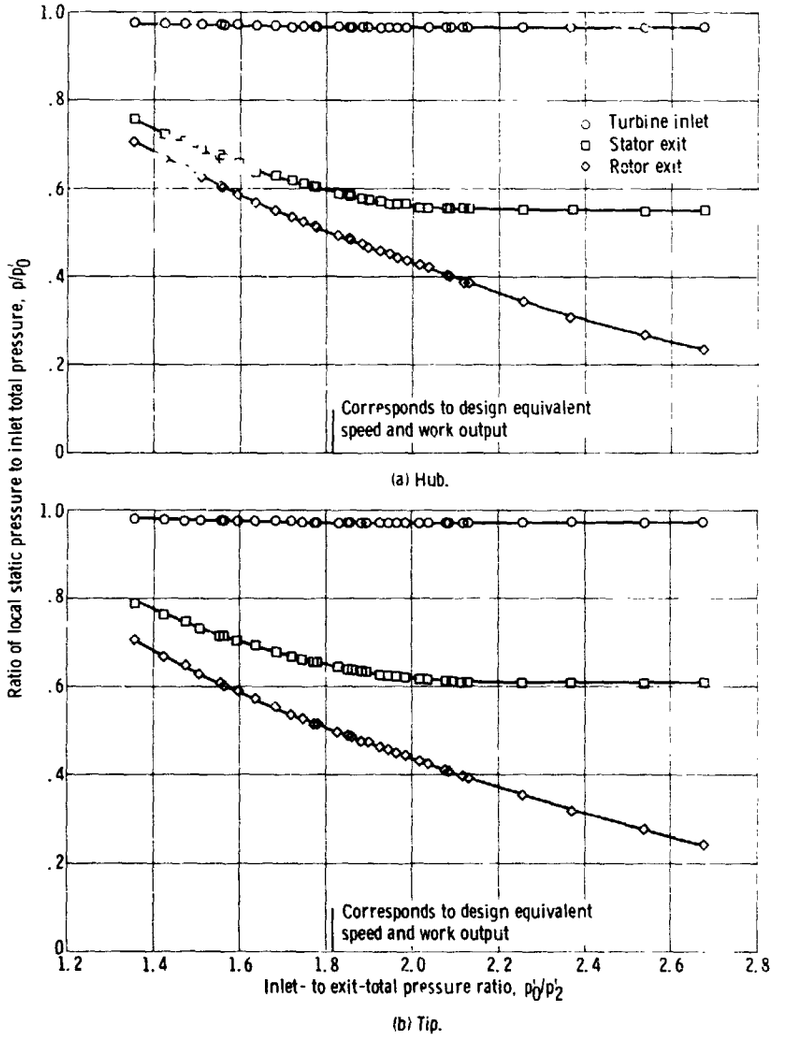

Figure 14. - Variation of static pressure through turbine with inlet- to exit-total pressure ratio at equivalent design speed for untwisted rotor configuration.

Turbine Performance With Twisted Rotor Blades

Overall performance. - The overall performance map for the turbine with twisted rotor blades is shown in figure 15 and is similar to that shown in figure 9 for the turbine with the untwisted blades. Over the range of speeds and pressure ratios investigated, the total efficiency of the turbine with untwisted rotor blades was less than the efficiency of the turbine with twisted rotor blades

At design speed and at a total pressure ratio of 1.817, the specific work output was 39.99 joules per kilogram (17.18 Btu/lbm). This corresponds to an efficiency of 88.0 percent.

Torque and mass flow characteristics. - The variation of equivalent torque $\epsilon\tau/\delta$ and of equivalent flow $\epsilon w\sqrt{\theta_{cr}}/\delta$ with pressure ratio for the speeds investigated is shown in

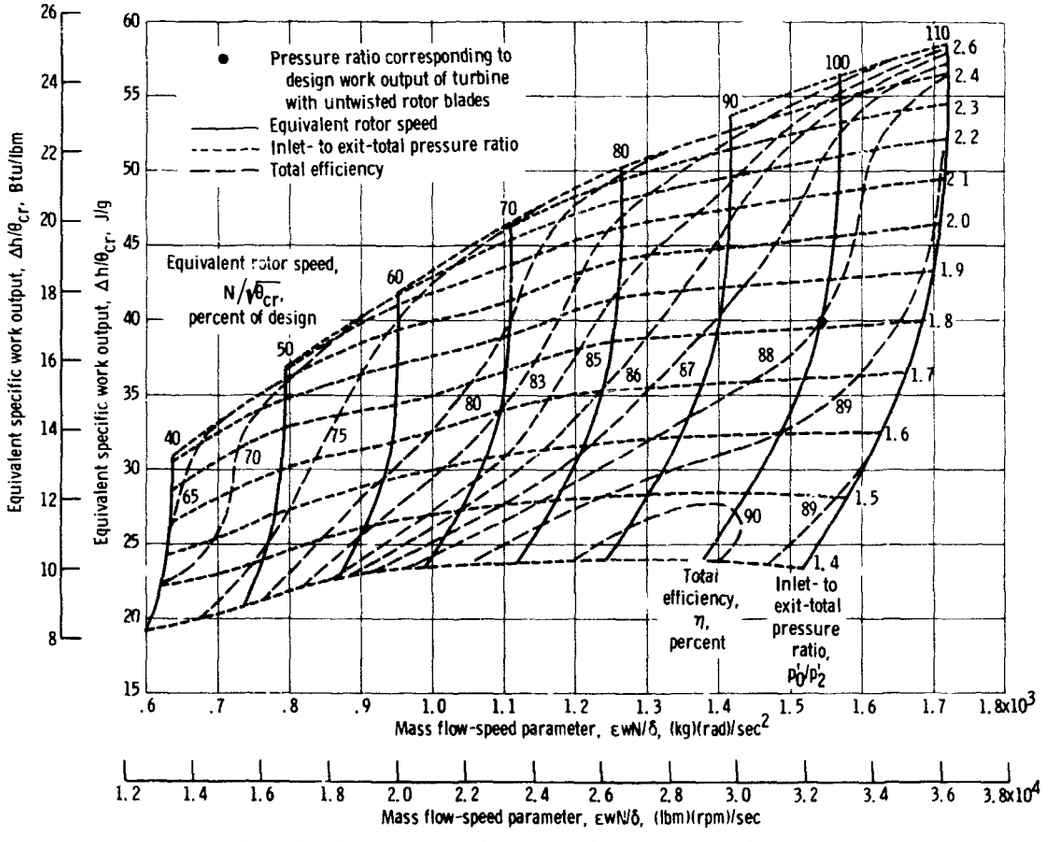

Figure 15 - Overall turbine performance map for turbine with twisted rotor blades.

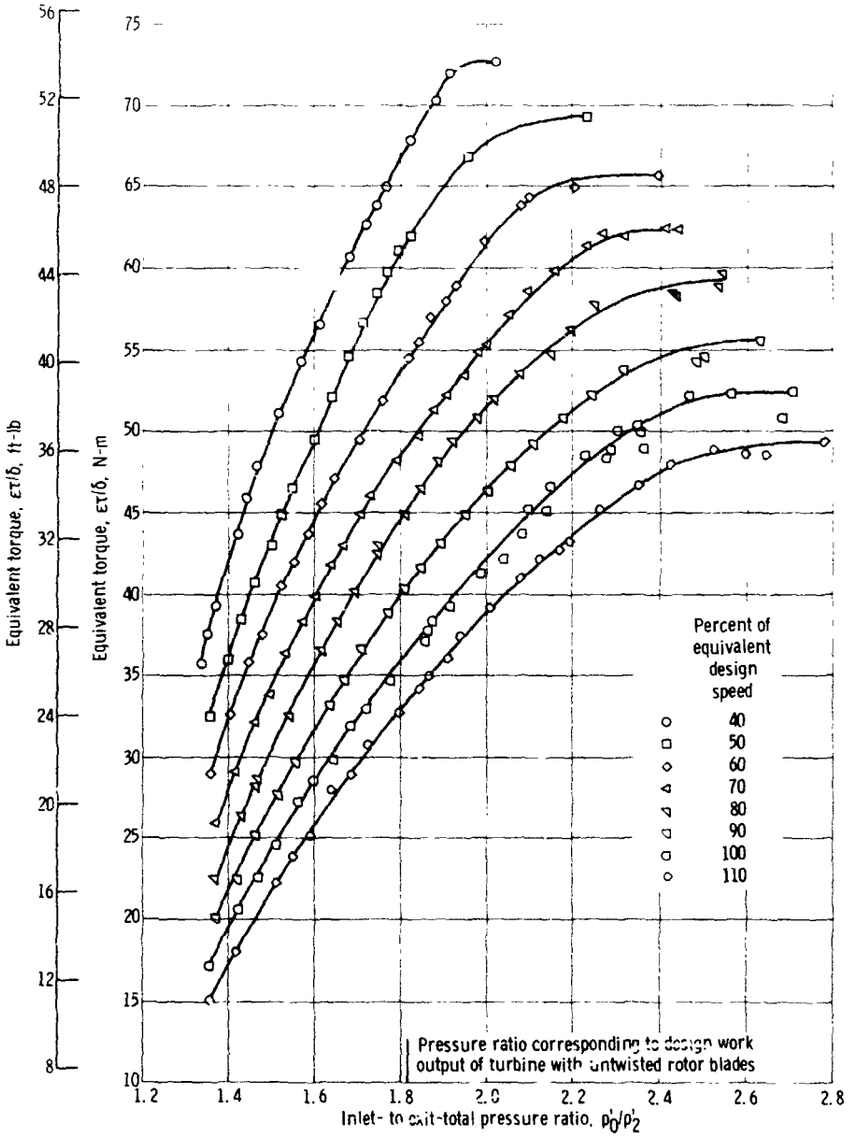

Figure 16. - Variation of torque with pressure ratio and speed for twisted rotor blade configuration.

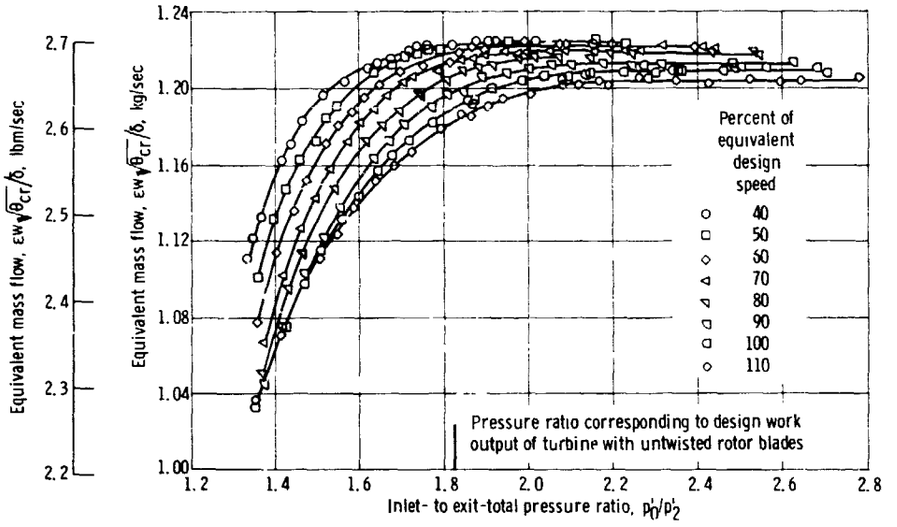

Figure 17. - Variation of mass flow with pressure ratio and speed for twisted rotor blade configuration.

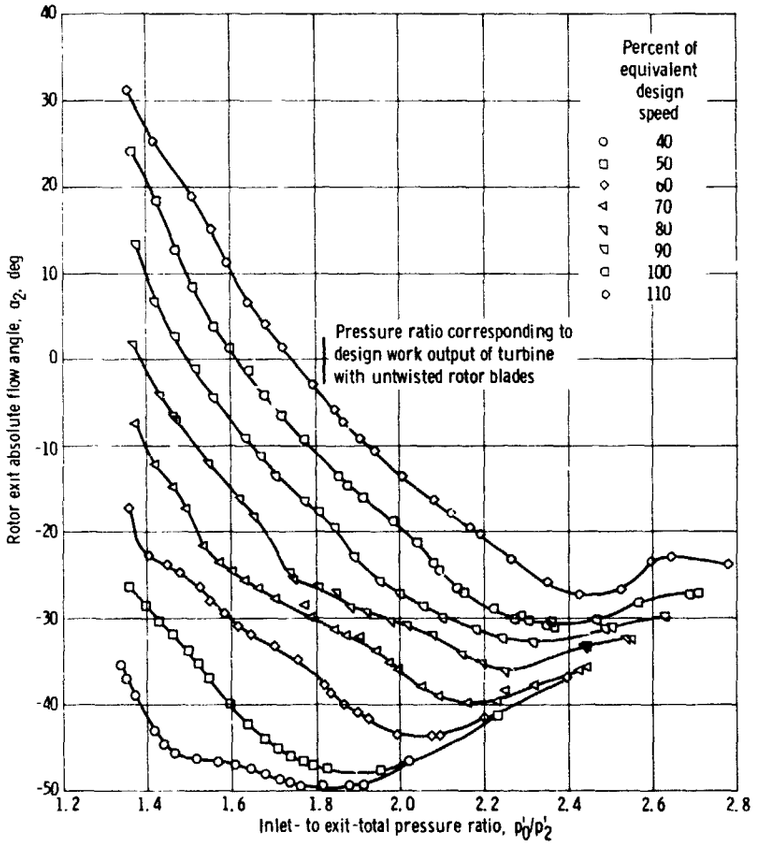

Figure 18. - Variation of turbine exit absolute flow angle with pressure ratio and speed for twisted rotor blade configuration.

figures 16 and 17, respectively. These curves are similar in trend to those obtained with untwisted rotor blades.

At the design equivalent speed and at a pressure ratio of 1.817, the equivalent mass flow was 1.189 kilograms per second (2.621 lbm/sec). The corresponding equivalent torque was 36.607 newton-meters (27.00 ft-lb).

The turbine outlet flow angle data are presented in figure 18; the static pressure distribution through the turbine for the design speed is shown in figure 19. These data have the same trends as found for the turbine with the twisted rotor blades (figs. 13 and 14) and are included for completeness.

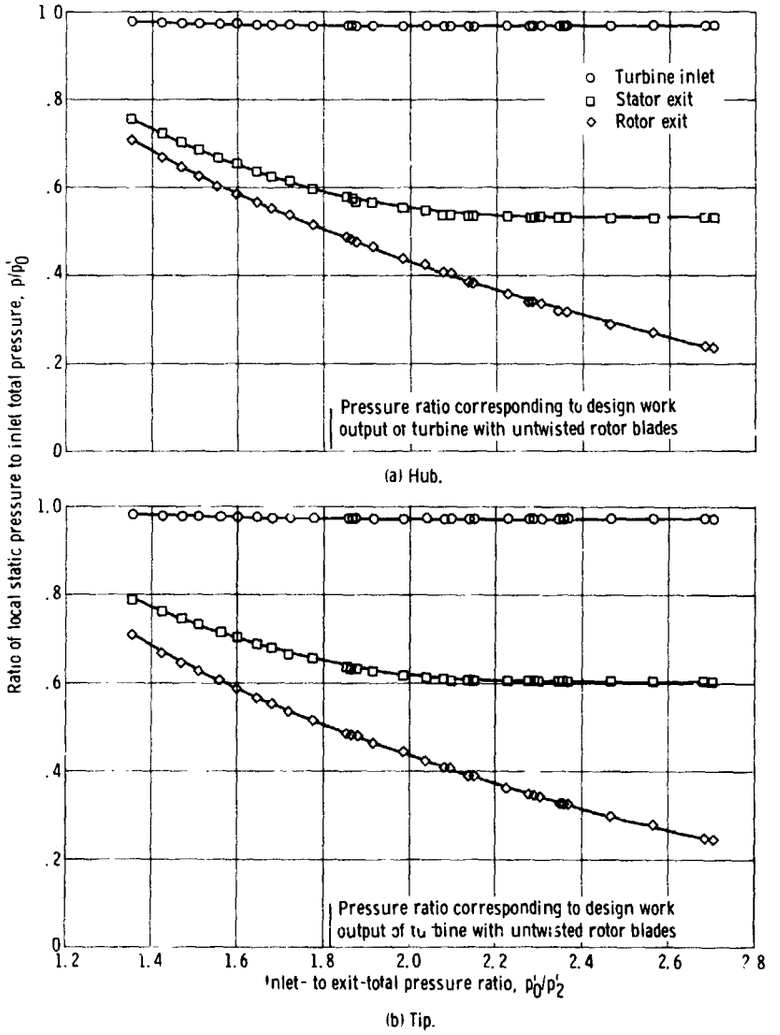

Figure 19. - Variation of static pressure through turbine with inlet- to exit-total pressure ratio at equivalent design speed for twisted rotor configuration.

Turbine Performance Comparison

A comparison of total efficiency between the turbine with the untwisted rotor blades and the turbine with twisted rotor blades is shown in figure 20. At a pressure ratio of 1.817, the efficiency of the turbine with the untwisted rotor blades was 87.1 as compared to 88.0 percent for the turbine with the twisted rotor blades. The difference in efficiency is attributed to the difference in rotor inlet incidence angle between the two rotor configurations.

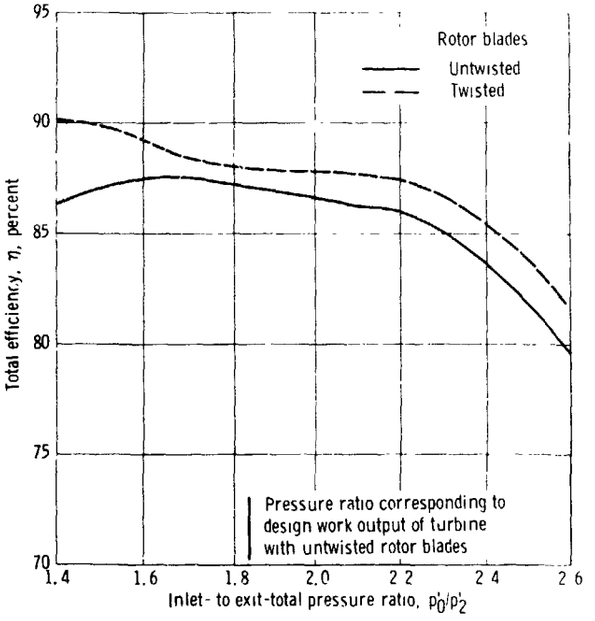

Figure 20. - Variation of total efficiency with inlet- to exit-total pressure ratio at equivalent design speed.

The incidence angles at the hub, mean, and tip sections as a function of overall total pressure ratio for the design speed are shown in figure 21 for the two rotor configurations tested. The incidence angles were determined by using the measured exit flow angle, calculating ΔV_u from the speed and specific work output and solving for the stator exit velocity by assuming a stator exit angle, and iterating until continuity at the rotor inlet was satisfied. A stator efficiency of 96 percent was assumed. Free-vortex flow at the stator exit was also assumed. This assumption was reasonable because of the high hub to tip ratio (0.85) and the small amount of twist necessary for a free-vortex design. At a pressure ratio of 1.817, the incidence angles for the untwisted rotor are approximately $+13.0^\circ$ at the hub, $+5.0^\circ$ at the mean, and -5.5° at the tip. Reference 1 indicates that the incidence at the mean and tip sections should not significantly affect turbine performance;

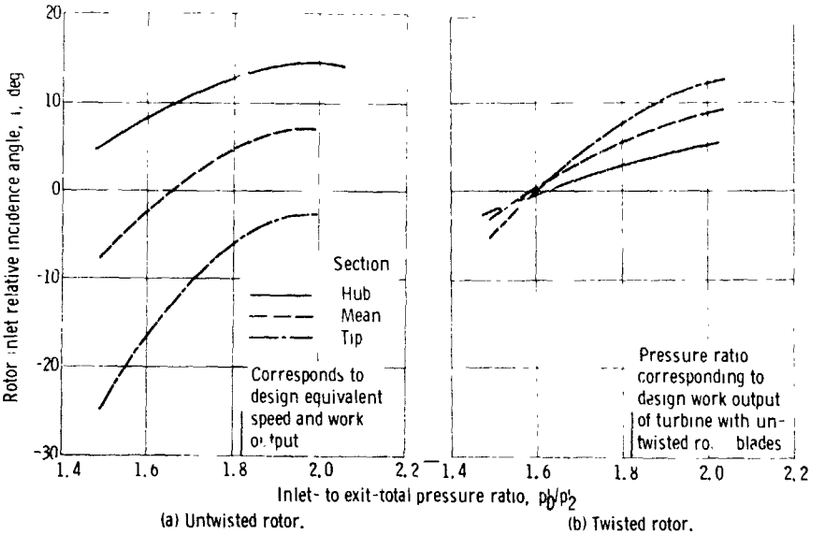

Figure 21. - Variation of rotor inlet relative incidence angle inlet- to exit-total pressure ratio.

however, the $+13.0^{\circ}$ at the hub section could result in some loss due to local flow separation. The reference shows the losses are dependent upon the amount of reaction across the rotor - the greatest losses occur with impulse turbines. The test results indicate that the $+13.0^{\circ}$ incidence did contribute to some loss since the efficiency did improve as the pressure ratio was reduced and a more favorable incidence angle was produced at the hub section (see fig. 20). As the pressure ratio was further reduced, the incidence angle at the tip was becoming highly negative, thus quickly offsetting any gain at the hub. The highest efficiency obtained for the untwisted rotor configuration was 87.5 percent at a pressure ratio of 1.65.

At a pressure ratio of 1.817, the incidence angles for the twisted rotor are $+8.5^{\circ}$ at the tip section, $+6.0^{\circ}$ at the mean section, and $+3.0^{\circ}$ at the hub section. As in the case for the untwisted rotor blade version, the large positive incidence may have contributed to some loss in turbine efficiency. This is evidenced by an increase in turbine efficiency as the pressure ratio was reduced below 1.817 (fig. 20), and the incidence angles approached zero. At pressure ratios below 1.6 the efficiency continued to increase indicating some negative incidence to be desirable. The turbine was not tested below a pressure ratio of about 1.4.

At pressure ratios above 1.817, the efficiency of both turbines decreased. This was due to an increase in positive incidence into the rotor. At a pressure ratio of approximately 2.1, both rotors choked and the incidence angle into the rotor for both configurations remained constant. The difference in efficiency between the two turbines beyond a pressure ratio of 2.1 is a constant 2 points and is attributed to the difference in incidence between the two turbines. The drop in efficiency as the pressure ratio increases is due

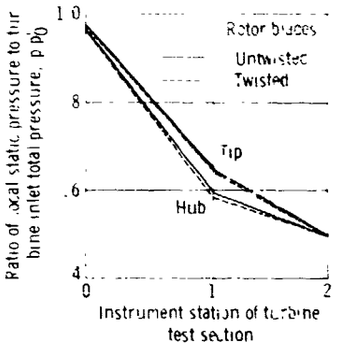

Figure 22. - Comparison of static pressure variation through turbine between turbine with untwisted rotor blades and turbine with twisted rotor blades.

to normal off-design effects.

The static pressure variations through the turbines are shown in figure 22. The static pressure distribution for both the untwisted and twisted rotors are approximately the same. The high radius ratio of the turbines (hub diameter to tip diameter) resulted in the small radial pressure gradients observed at the stator exit locations (station 1, fig. 22).

SUMMARY OF RESULTS

An experimental investigation of a turbine suitable for high-temperature "core" engine application was made to determine the performance level of the basic blading over a range of speed and pressure ratio, and the effect of using untwisted constant profile rotor blades rather than blades designed for free-vortex flow. All experimental data are for a solid, uncooled, half-scale version of the actual turbine. The pertinent results are as follows:

1. At the design equivalent speed of 12 388 rpm, the design specific work output of 39.57 joules per gram (17.00 Btu/lbm) was obtained at an overall total pressure ratio of 1.817 for the turbine with untwisted rotor blades. The corresponding efficiency was 87.1 percent. This agrees well with the design efficiency of 87 percent.

2. At the aforementioned pressure ratio the specific work output of the turbine with the twisted blades was 39.99 joules per gram (17.18 Btu/lbm) which results in an efficiency of 88.0 percent. Thus, an approximate one point loss was incurred by using untwisted rotor blades. The difference in efficiency between the two rotor configurations is attributed to the higher incidence losses of the untwisted rotor blade version.

3. The twist in the rotor blade had little effect on the flow capacity of the turbine. At

a pressure ratio of 1.817 the mass flows for the untwisted rotor blades and twisted rotor blades were 1.188 kilograms per second (2.620 lbm/sec) and 1.189 kilograms per second (2.621 lbm/sec), respectively. The design flow was 1.207 kilograms per second (2.660 lbm/sec).

4. The turbine efficiency obtained agreed well with the predicted design efficiency which factored in corrections for low aspect ratio, Reynolds number effects, and large radial clearances.

Lewis Research Center,
National Aeronautics and Space Administration,
Cleveland, Ohio, September 24, 1973,
501-24.

REFERENCES

1. Ainley, D. G.; and Mathieson, G. C. R.: An Examination of the Flow and Pressure Losses in Blade Rows of Axial-Flow Turbines. Rep. R&M 2891, Aeronautical Research Council, Gt. Britain, 1955.

2. Katsanis, Theodore: FORTRAN Program for Calculating Transonic Velocities on a Blade-to-Blade Stream Surface of a Turbomachine. NASA TN D-5427, 1969.

NASA-Langley, 1974 E-7592